Interchange reconnection within coronal holes powers the fast solar wind

S. D. Bale[1, 2], J. F. Drake[3,4], M. D. McManus[1,2], M. I. Desai[5], S. T. Badman[1,2], D. E. Larson[2], M. Swisdak[3], N. E. Raouafi[6], T. Phan[2], M. Velli[7], D. J. McComas[8], C. M. S. Cohen[9], D. Mitchell[6], O. Panasenco[10], J. C. Kasper[11,12]

[1]Physics Department, University of California, Berkeley, CA, USA
[2]Space Sciences Laboratory, University of California, Berkeley, CA, USA
[3]Department of Physics, the Institute for Physical Science and Technology and the Joint Space Institute, University of Maryland, College Park, MD, USA
[4]Institute for Research in Electronics and Applied Physics, University of Maryland, College Park, MD, USA
[5]Southwest Research Institute, San Antonio, TX, USA
[6]Johns Hopkins Applied Physics Laboratory, Laurel, MD, USA
[7]Department of Earth, Planetary, and Space Sciences, University of California, Los Angeles, CA, USA
[8]Department of Astrophysical Sciences, Princeton University, Princeton, NJ, USA
[9]California Institute of Technology, Pasadena, CA, USA
[10]Advanced Heliophysics Inc., Los Angeles, CA, USA
[11]BWX Technologies, Inc., Washington, DC, USA
[12]Climate and Space Sciences and Engineering, University of Michigan, Ann Arbor, MI, USA

The fast solar wind that fills the heliosphere originates from deep within regions of open magnetic field on the Sun called 'coronal holes'. However the energy source responsible for accelerating the outflowing plasma to such high speeds is still widely debated, although there is broad evidence that it is ultimately magnetic in nature with candidate mechanisms including Alfven wave heating[1,2] and interchange reconnection[3,4]. The magnetic field near the solar surface within coronal holes is structured on spatial scales associated with the boundaries of meso-scale supergranulation convection cells, where descending flows create intense bundles of magnetic field. The energy density in these 'network' magnetic field bundles is a likely candidate as an energy source of the wind. Here we report measurements of two fast solar wind streams from the Parker Solar Probe (PSP) spacecraft[5] near its 10th perihelion which provides strong evidence for the interchange reconnection mechanism. Specifically, we show that supergranulation structure at the coronal hole base remains imprinted in the near-Sun solar wind resulting in asymmetric patches of magnetic ``switchbacks''[6,7] and bursty solar wind streams with corresponding energetic ions with power law-like distributions extending to beyond 100 keV. Particle-in-cell simulations of interchange reconnection between open and closed magnetic structures support key features of the observations, including the energetic ion spectra. Important characteristics of interchange reconnection in the low corona are inferred from the PSP data including that the reconnection is collisionless and that the rate of energy release is sufficient to heat the ambient plasma and drive the fast wind. In this reconnection scenario of solar wind energization, open magnetic flux undergoes continuous reconnection and the wind is driven both by the resulting plasma pressure and the radial Alfvenic flow bursts.

Recent measurements from the NASA Parker Solar Probe (PSP) revealed that the solar wind emerging from coronal holes, or 'streams,' is organized into 'microstreams' with an angular scale (5-10°) in Carrington longitude[8] similar to the underlying supergranulation cells associated with horizontal flows in the photosphere[9]. Supergranulation flows are thought to drag the photospheric magnetic field into the convective downflows where the field intensifies and the magnetic field energy density dominates over the plasma pressure[2]. However, the footpoints of the previous PSP encounter were inferred to be at high latitudes on the far side of the Sun so that the detailed magnetic structure of the cells and their connectivity to the spacecraft could not be determined, preventing a complete analysis of the source of these wind microstreams.

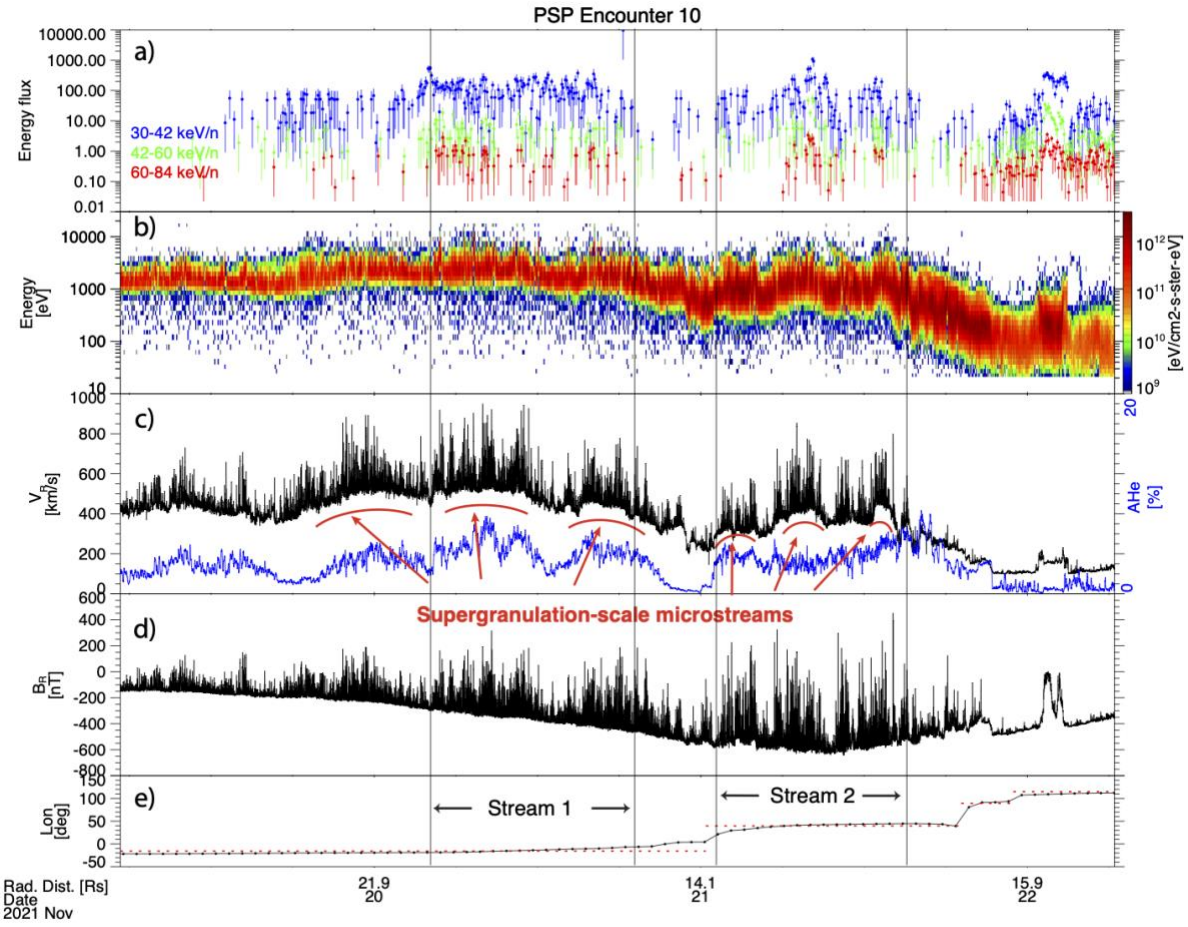

Fig 1. **Time series measurements of the solar wind plasma and magnetic field through the November 2021 solar encounter**. a. Hot solar wind ions extend in energy to ~85keV as suprathermal tails on the proton particle distribution in (b). c. Red arcs mark the solar wind radial velocity microstream structure that is organized in Carrington longitude at angular scales associated with supergranulation convection and the photospheric network magnetic field (see Fig. 2). These microstreams become shorter in duration as the spacecraft accelerates through perihelion near the center of this figure and sweeps more rapidly through Carrington longitude. The thermal alpha particle abundance (blue trace in panel c) is similarly modulated by the microstream structure. The alpha particle abundance is frozen-in at the base of the corona. (d) Reversals of the radial magnetic field, so-called 'switchbacks',

are organized by the microstreams and are linked to the radial flow bursts by the Alfvenicity condition). (e). Photospheric footpoints from a PFSS model instantiation indicate two distinct coronal hole sources well-separated in Carrington longitude, shown in Fig 2 (and as dotted lines in Fig. 1e)

Microstream velocity structure formed at the base of the corona

On solar Encounter 10 (E10) the PSP came within 12.3 solar radii (R_S) of the photosphere in late November 2021. Figure 1 summarizes the plasma[10], energetic ion[11] and magnetic field measurements[12] made near perihelion during E10. A spectrogram of ions in Fig. 1a and 1b extends from thermal energies to ~85 keV and, like the proton velocity in Fig. 1c, is structured as discrete 'microstreams'[13,14,8] whose duration decreases from ~10 hours to ~2 hours as the spacecraft approaches perihelion on 08:25 Nov 21, 2021. Data presented in Fig. 4b (and discussed later in greater detail) reveals that the wind ion energy distributions are power laws at high energy that extend to greater than 100 keV. The characteristic structure of the microstreams is highlighted by red arcs in Fig. 1c and a blue trace indicates the measured thermal alpha particle abundance $A_{He} = n_\alpha/n_p$ which is similarly modulated. The high First Ionization Potential (FIP) of Helium requires that the alpha particle abundance is frozen-in at very low altitudes in the corona or in the chromosphere at the base of the wind[15], so these microstream structures are organized at the source of the wind itself. The radial component of the measured interplanetary magnetic field in Fig. 1d shows that large-amplitude, Alfvenic field reversals, that have been termed 'switchbacks', are also associated with the microstreams. A Potential Field Source Surface (PFSS) model[16-18] [see Supplementary Information] of the coronal magnetic field is used to infer the footpoints of the magnetic field that connects to the PSP spacecraft and reveals the connection to two separate near-equatorial coronal holes. The time series of the longitude of the footpoint on the solar surface is shown in Fig. 1e and as white diamonds against a 193Å SDO/EUV[19] image in Figure 2.

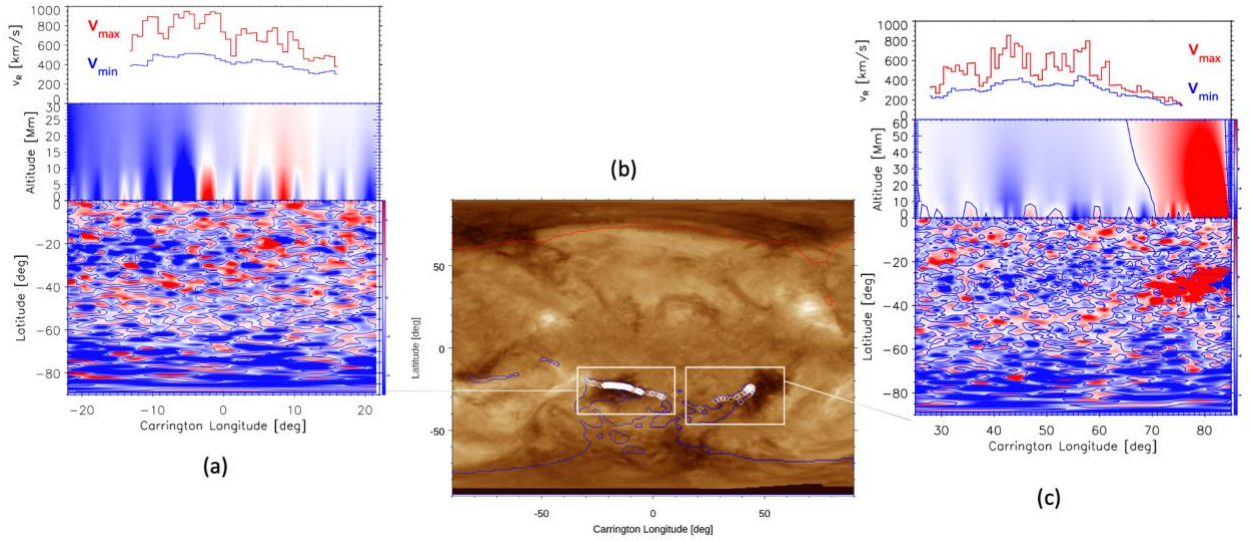

Fig 2. Solar wind during PSP Encounter 10 emerges from two coronal holes. An extreme ultraviolet (193Å) map of the corona shows cooler regions (darker pixels) associated with open magnetic field within two separate, near-equatorial coronal holes. A PFSS model maps the interplanetary magnetic field from the PSP spacecraft to footpoints (white diamonds) within the coronal holes. Panel (A) shows the magnetic field and velocity microstream profile within the first coronal hole: the upper panel shows minimum (blue) and maximum (red) radial speed vs longitude, while the 2nd panel shows the vertical magnetic field along the footpoints extending from the photosphere to 30 Mm from magnetogram measurements and a PFSS model that accounts for the motion of the spacecraft. The bottom panel is a map of the magnetic field polarity just above the photosphere, again from the PFSS model. The panel at right shows the corresponding structure within the 2nd coronal hole. These data indicate that the radial magnetic field is organized into mixed radial polarity intervals on the same scales as the velocity micro-streams observed by PSP.

The linkage of the temporal structure of the switchback and radial velocity bursts with the spatial periodicity of the surface magnetic field documented in Figs. 1 and 2 suggests the possibility that magnetic reconnection between open and closed magnetic fields in the low corona (interchange reconnection) is the driver of these bursts[8]. Consistent with the observations, interchange reconnection in the weakly collisional corona is expected to be bursty rather than steady[20-23]. The energetic ions and enhanced pressure in these burst intervals are also signatures of reconnection[24-26] and further support the reconnection hypothesis as the source of these bursts. If reconnection is the driver of these bursts, the data suggests that interchange reconnection is a continuous process in the source regions of open flux. Figure 3c is a schematic (in 2D for simplicity) that shows open flux reconnecting with closed flux regions in the low corona (see the caption for a detailed description). In this figure the open flux migrates to the left, reconnecting with successive regions of closed flux with the consequence that the bursty outflow from interchange reconnection fills all of the open flux as seen in the data.

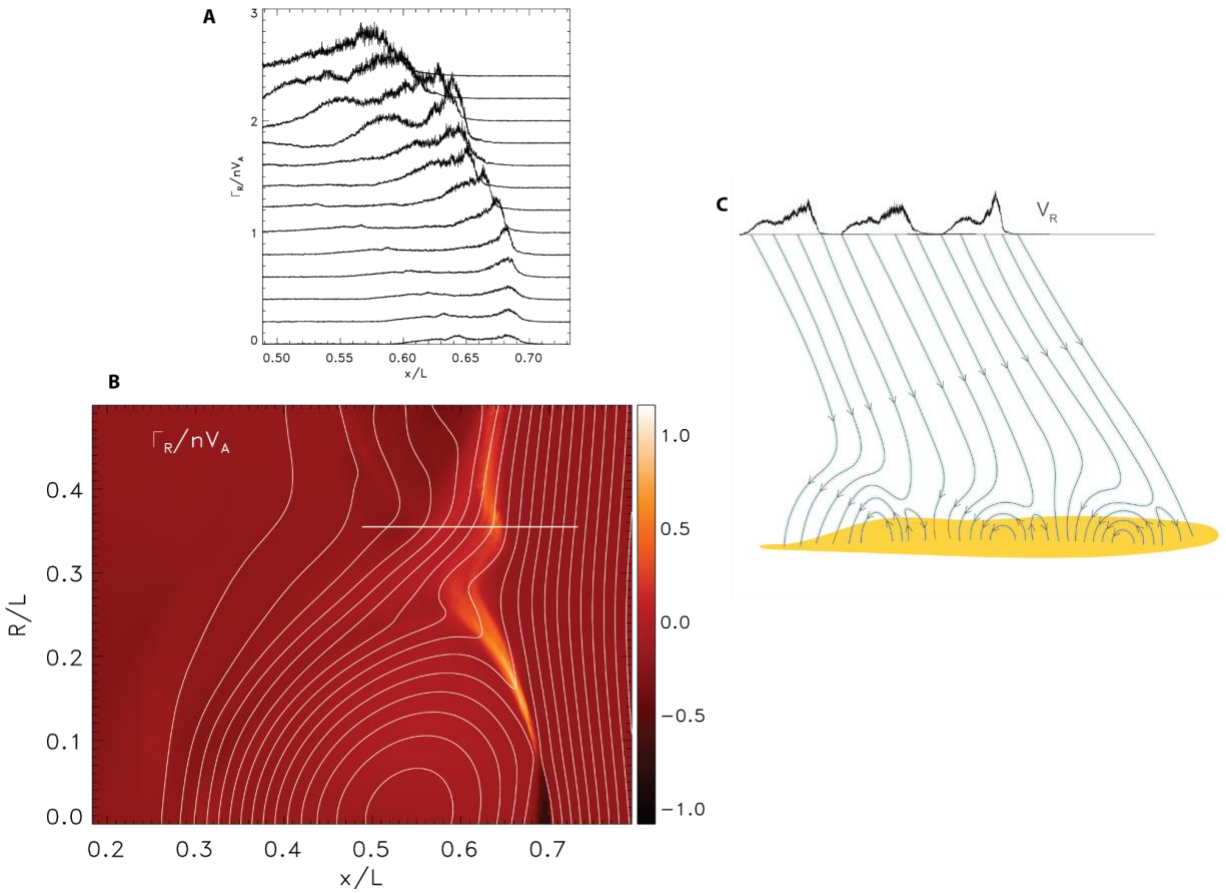

Figure 3: Schematic of interchange reconnection and the structure of the reconnection exhaust from a simulation. In (c) a schematic of reconnection between open and closed magnetic flux (interchange reconnection) in the low corona based on the PSP data shown in Figure 1. The data suggests that reconnection between open and closed flux is nearly continuous. In the schematic the open magnetic flux is moving continuously to the left. An open field line first reconnects with the closed flux above the solar surface, forming upward and downward oriented loops. The open bent field then straightens and drives Alfvenic flow outward. As it moves to the left, the open field line then intersects another closed flux region and the process repeats. Thus, the open flux is completely filled with high-speed outflowing plasma – the exhaust from interchange reconnection. The cuts of the radial velocity measured by an observer crossing the open flux at the top of the schematic indicate that the highest speed bursty outflows are on newly reconnected magnetic fields while on field lines that reconnected earlier, the highest speed flows have already passed by the observation location. This time asymmetry was clear in the E06 data[8]. In (b) the radial particle flux with overlying magnetic fields in white from a particle-in-cell (PIC) simulation of interchange reconnection showing Alfvenic upward and downward flows from the reconnection site above the coronal surface. Details about the simulation setup are found in the Supplementary material. The reconnected magnetic field migrates to the left as it straightens and drives the outflow exhaust. Shown in (a) is a time sequence of the radial flux along the cut shown by the horizontal white line in (b). Each successive cut is separated by a time 0.037 L/V_A, with L/V_A the Alfven transit time across the simulation domain, and is shifted upward to avoid overlapping the data. The cuts reveal the bursty nature of the outflow resulting from the generation of flux ropes within the elongated current layer[20-23]. As shown in the schematic, newly reconnected field lines have higher outflow fluxes than field lines reconnected earlier in time.

Interchange Reconnection

To establish that interchange reconnection is the source of the bursty radial flows, we use the observational data combined with well-established principles of reconnection to deduce the

basic characteristics of reconnection in the low corona. The strength of the magnetic field undergoing reconnection is a key parameter. Since the magnetic field strength at the base of the corona has significant variation, we estimate the amplitude of the reconnecting magnetic field by projecting the measured magnetic field at PSP back to the solar surface. The usual R^{-2} falloff of the radial magnetic field with radius R is valid in the solar wind, but fails closer to the Sun. . Thus, we use a combination of the R^{-2} behavior at large R with a falloff derived from a surface averaged PFSS model below 2.5 R_s (see Supplementary Material.) The resulting projection of the 600 nT magnetic field at 13.4 R_s to the low corona is 4.5 G, which is consistent with the PFSS data in Fig. 2.

The plasma density undergoing reconnection at the base of the corona is not measured directly. However, the characteristic amplitude of the bursty flows at PSP are around 300km/s. Since the flows during bursty reconnection are Alfvenic, we can estimate the density knowing the magnetic field strength. The resulting density is around $10^9/cm^3$, which is again a reasonable value for the low corona[27].

To address whether the rate of energy release during reconnection is sufficient to drive the wind requires an estimate for the reconnection inflow rate V_r. A lower limit for the rate follows from the fact that the flow bursts are nearly continuous. To see this, we define the reconnection time $t_r = L_B/V_r$, the time required for open field lines to traverse the characteristic scale length L_B of the surface magnetic field, which is around 10^o or 6×10^4 km. A second time is the time $t_b \sim R_{PSP}/V_R$ for the reconnection bursts to reach the spacecraft at R_{PSP}. In the limit $t_r >> t_b$, the outflows from the reconnection site in the corona would quickly pass by the spacecraft and there would be no high speed flows until the spacecraft connected to another reconnection site in the corona. When $t_r \le t_b$, the spacecraft would measure bursty flows as the spacecraft crossed the entire supergranulation scale. The observations reveal the latter since bursty flows are measured during the entire crossing of the supergranulation scale. Thus, the observations suggest that $t_r \sim t_b$ or $V_r \sim L_B V_R/R_{PSP} \sim 30$ km/s or around 0.1 of the local Alfven speed, a reasonable value if reconnection is collisionless[28-30] but somewhat faster than the MHD prediction[31]. However, for the parameters of reconnection just calculated and with ambient temperatures of around 100 eV the reconnection electric field is around four orders of magnitude above the Dreicer runaway field. In this regime classical collisions are too weak to limit electron acceleration and collisionless processes dominate. Interchange reconnection driving the bursty flows measured by PSP is therefore collisionless and the rate of reconnection is consistent with expectations.

The rate of magnetic energy release from interchange reconnection is given by $V_r B^2/4\pi \sim 5\times10^5$ ergs/cm^{2}sec using B = 4.5 G and V_r = 30 km/s. This is comparable to that required to drive the high speed wind, which is around 10^5–10^6 ergs/cm^{2}sec[1].

Thus, we have established through the PSP observations, the SDO/HMI surface magnetic field measurements and well-established characteristics of magnetic reconnection that interchange reconnection is sufficient to drive both the ambient base solar wind flow (through the pressure increase of the ambient plasma) as well as the strong magnetically driven flow bursts that lie on top of this flow. Specifically, the base solar wind is driven by the usual radial pressure drop[1] as well as the exospheric processes[32] associated with strong electron heating. Further tests of the interchange reconnection explanation of the microstream structure of the wind measured at PSP concerns the structuring of the flow bursts and the production of energetic protons and alphas. A key observation reported in the E06 data[8] and illustrated in the schematic in Fig. 3c is the time

asymmetry in the burst amplitudes: large amplitude bursts onset sharply and gradually decrease in amplitude across the burst period and the time sequence then repeats. Data from a particle-in-cell (PIC) simulation of interchange reconnection is presented in Fig. 3b (See also the Supplementary material). A cut across the outflow simulation exhaust reveals high speed bursts on newly reconnected field lines in the exhaust adjacent to the magnetic separatrix while on field lines in the exhaust interior, the fastest flow bursts have already passed the location of the cut so the measured flows are weaker (Figure 3a). Thus, the simulations support the hypothesis that the bursts observed by PSP correspond to crossings of interchange reconnection exhausts. Such dispersion signatures have been well documented in the cusp region of the Earth's magnetosphere as a result of reconnection at the terrestrial magnetopause[33]. Reconnection between the closed magnetic flux of the Earth and "open" flux in the solar wind is a clear analogue of coronal interchange reconnection.

Finally, the spectrum of energetic protons and alphas has been calculated from the interchange reconnection simulations. The simulation includes fully stripped alpha particles that are 5% by number, close to that expected in the solar atmosphere[15]. The spectrum of the energy flux of both species is shown in Fig. 4a. This data is taken from the outflow exhaust and so includes only plasma that has undergone acceleration either near the x-line or on entry into the exhaust. Both the protons and alphas exhibit an energetic, non-thermal powerlaw distribution with spectral indices of around -7 for both species. As shown in Fig. 4b, the spectrum of the differential energy flux of particles during the time interval 04:00-19:00 Nov 20, 2021 from Fig. 1, there are also energetic protons and alphas during the switchback bursts with energies up to around 100 keV. The spectra are again rather soft, having spectral indices of around -7, consistent with the simulation data. The energy in the simulation is normalized to the free parameter $m_iV_A^2$. By equating the energy minimum of the proton powerlaw in the simulation (~3.6 $m_iV_A^2$) to that of the SPAN data (~5 keV), we find that the coronal value of $m_iV_A^2$ is around 1.4 keV compared with around 0.9 keV from the 300 km/s estimate for V_A based on the amplitude of the bursty flows measured by SPAN at 13.4 R_s. That the two values of $m_iV_A^2$ are close indicates that the Alfven speed in the corona where reconnection is taking place is in the range of 300 to 400 km/s.

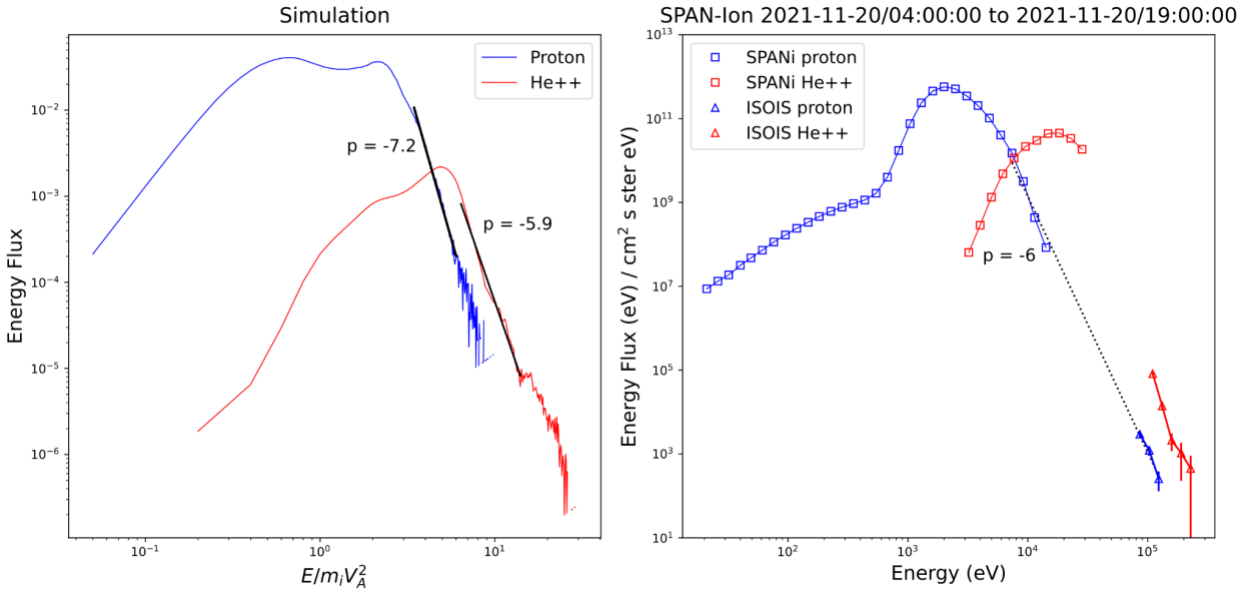

Fig. 4. Proton and alpha particle differential energy flux from interchange reconnection simulations and solar wind observations. In (a) the proton (blue) and alpha particle (red) energy fluxes taken from the outflow exhaust from an interchange reconnection simulation (see Supplementary section for simulation details). The energy normalization in the simulation is $m_iV_A^2$, which is an arbitrary parameter[34]. The units in the vertical direction are arbitrary although the reduced height of the alpha flux reflects the 5% number density of alphas. Both fluxes peak and then roll over into distinct soft powerlaws with slopes of -7.2 and -5.9 for the protons and alphas respectively with the alpha spectrum shifted to higher energy compared with that of the protons. In (b) the proton (blue) and alpha (red) energy fluxes from SPANi and ISOIS during the time interval 04:00:00-19:00:00 Nov 20, 2021 from Fig. 1. As in the simulations, the spectra peak and roll over into powerlaw-like suprathermal tails with similar slopes of -7 and -6 for the protons and alphas, respectively. Thus, the powerlaw slopes from the simulation and the observational data are very close. The SPANi data for the alphas does not extend to high enough energy to capture any powerlaw behavior. The shift to higher energy of the alpha spectrum compared with the protons in the observations exceeds that from the simulation. Finally, we can use the low energy bound of the powerlaw distribution from the simulation (~3.6 $m_iV_A^2$) and observations (~5keV) to establish that the value of $m_iV_A^2$ at the coronal reconnection site is around 1.4keV. This is comparable with around 0.9keV from the 300km/s estimate for V_A based on the amplitude of the burstyflows measured by SPAN at 13.4R_S.

Discussion

The PSP measurements from E10 show that the radial solar wind velocity is modulated on a scale that corresponds to polarity inversions of the surface magnetic field within coronal holes. The modulations are characterized by strong radial flow bursts that are expected from turbulent, collisionless reconnection in the coronal environment. Since the rate of energy release inferred from the PSP data, is sufficient to drive the wind, the picture that emerges is that reconnection heats the ambient coronal plasma necessary to drive the bulk outflow[35] and produces the turbulent fluctuations that ride this outflow[20-23]. An alternate interpretation might have been that the magnetic energy release from reconnection drives Alfven wave turbulence that ultimately heats the ambient plasma to drive the bulk outflow[36,1,2]. However, the evidence against such a hypothesis is that the time asymmetry that characterizes the bursty flows[8] and the spectral indices of the powerlaw distributions of energetic protons and alphas measured in the data are in remarkably good agreement with the interchange reconnection simulation data and are unique to the reconnection scenario. These distinctive measurements and supporting

analysis demonstrate that interchange reconnection is the likely energy source of the fast solar wind.

Acknowledgments: The FIELDS, SWEAP, and ISOIS suites were designed, developed, and are operated under NASA contract NNN06AA01C. We acknowledge the extraordinary contributions of the PSP mission operations and spacecraft engineering team at the Johns Hopkins University Applied Physics Laboratory.

Author contributions: S.D.B. wrote the manuscript with major contributions from J.F.D. and S.T.B. S.D.B. analyzed the PSP measurements, with contributions from M.D.M, M.I.D., and D.E.L. S.T.B. performed the PFSS analysis. J.F.D. and M.S. performed the computer simulations. S.D.B, J.C.K., and D.J.M. lead the PSP/FIELDS, SWEAP, and ISOIS teams respectively. All authors participated in the data interpretation and read and commented on the manuscript.

Data availability: The PSP data used in this study are available at the NASA Space Physics Data Facility (SPDF).

References

1. McKenzie, J. F., M. Banaszkiewicz, and W. I. Axford, Acceleration of the high speed solar wind, Astron. Astrophys., 303, L45 (1995).
2. Axford, W. I. et al., Acceleration of the high speed solar wind in coronal holes, Space Science Rev., 98, 25 (1999).
3. Fisk, L. A., N. A. Schwadron, and T. H. Zurbuchen, Acceleration of the fast solar wind by the emergence of new magnetic flux, J. Geophys. Res., 104, A9, 19765 (1999).
4. Cranmer, S. R. and A. A. van Ballegooijen, Can the solar wind be driven by magnetic reconnection in the Sun's magnetic carpet, Astrophys. J., 720, 824 (2010).
5. Fox, N. J. et al., The Solar Probe Plus mission: Humanity's first visit to our star, Space Science Rev., 204, 7 (2016).
6. Bale, S. D. et al, Highly structure slow solar wind emerging from an equatorial coronal hole, Nature, 576, 237 (2019).
7. Kasper, J. C. et al., Alfvenic velocity spikes and rotational flows in the near-Sun solar wind, Nature, 576, 228 (2019).
8. Bale, S. D. et al, A solar source of Alfvenic magnetic field switchbacks: in situ remnants of magnetic funnels on supergranulation scales, Astrophys. J., 923, 174 (2021).
9. Rieutord, M., Rincon, F. The Sun's Supergranulation. *Living Rev. Sol. Phys.* 7, 2 (2010)
10. Kasper, J. C. et al., Solar wind electrons alphas and protons (SWEAP) investigation: design of the solar wind and coronal plasma instrument suite for Solar Probe Plus, Space Science Rev., 204, 131 (2016).
11. McComas, D. J. et al., Integrated Science Investigation of the Sun (ISIS): Design of the energetic particle investigation, Space Science Rev., 204, 187 (2016).
12. Bale, S. D. et al., The FIELDS instrument suite for Solar Probe Plus: Measuring the coronal plasma and magnetic field, plasma waves and turbulence, and radio signatures of solar transients, Space Science Rev., 204, 49 (2016).

13. Thieme, K. M., E. Marsch, and R. Schwenn, Spatial structures in high-speed streams as signatures of fine structures in coronal holes, Ann. Geophys., 8, 713 (1990).
14. Neugebauer, M. et al., Ulysses observations of microstreams in the solar wind from coronal holes, J. Geophys. Res., 100, A12, 23389 (1995).
15. Kasper J. C. et al., Solar wind helium abundance as a function of speed and heliographic latitude: variation through a solar cycle, Astrophys. J., 660, 901 (2007).
16. Schatten, K. H., J. M. Wilcox, and N. F. Ness, A model of interplanetary and coronal magnetic fields, Solar Phys., 6, 442 (1969).
17. Altschuler, M. D. and G. Newkirk, Magnetic fields and the structure of the solar corona. 1: Methods of calculating coronal fields, Solar Phys. 9, 131 (1969).
18. Hoeksema, J. T., Structure and evolution of the large scale solar and heliospheric magnetic fields, PhD thesis, Stanford Univ (1984).
19. Lemen, J. R. et al., The Atmospheric Imaging Assembly (AIA) on the Solar Dynamics Observatory (SDO), Solar Phys., 275, 17 (2012).
20. Drake, J. F. et al, Formation of Secondary Islands During Magnetic Reconnection, Geophys. Res. Lett., 33, 13015, (2006).
21. Bhattacharjee, A. et al., Fast reconnection in high-Lundquist-number plasmas due to the plasmoid Instability, Phys. Plasmas, 16, 11, 112102, (2009).
22. Cassak, P. A., M. A. Shay, and J. F. Drake, Scaling of Sweet-Parker reconnection with secondary islands, Phys. Plasmas, 16, 12, 120702 (2009).
23. Daughton, W. et al. Transition from collisional to kinetic regimes in large-scale reconnection layers, Phys. Rev. Lett., 103, 065004 (2009).
24. Drake, J. F. et al., Ion heating resulting from pickup in magnetic reconnection exhausts, J. Geophys. Res., 114, A5, A05111 (2009).
25. Drake, J. F., M. Swisdak, and R. Fermo, The power-law spectra of energetic particles during mulit-island magnetic reconnection, Astrophys. J. Lett., 763, L5 (2013).
26. Zhang, Q., F. Guao, and W. Daughton, Efficient nonthermal ion and electron acceleration enabled by the flux-rope kink instability in 3D nonrelativistic magnetic reconnection, Phys. Rev. Lett., 127, 185101 (2021).
27. Cranmer, S. R. et al., An empirical model of a polar coronal hole at solar minimum, Astrophys. J., 511, 481 (1999).
28. Shay, M. A. et al, The scaling of collisionless magnetic reconnection for large systems, Geophys. Res. Lett., 26, 2163 (1999).
29. Shay, M. A., J. F. Drake, and M. Swisdak, Two-scale structure of the electron dissipation region during collisionless magnetic reconnection, 99, 155022 (2007).
30. Daughton, W. et al., Computing the reconnection rate in turbulent kinetic layers by using electron mixing to identify topology, Phys. Plasmas, 21, 5, 052307 (2014).
31. Huang, Y.-M. and A. Bhattacharjee, Turbulent magnetohydrodynamic reconnection mediated by the plasmoid instability, Astrophys. J., 818, 20 (2016).
32. Halekas, J. S. et al., The radial evolution of the solar wind as organized by electron distribution functions, ArXiv, 2207.06563 (2022).
33. Burch, J. L. et al., Plasma injection and transport in the mid-latitude polar cusp, Geophys. Res. Lett., 9, 921 (1982).

34. Drake, J. F. et al., Switchbacks as signatures of magnetic flux ropes generated by interchange reconnection in the corona, Astron. Astrophys., 650, A2 (2021).
35. Parker, E. N., Dynamics of interplanetary gas and magnetic fields, Astrophys. J., 128, 664 (1958).
36. Axford, W. I. and J. F. McKenzie, The origin of high speed solar wind streams, Solar Wind Seven, 1 (1992).

Supplementary material

Supplementary: Potential Field Source Surface modeling

To generate the footpoints shown in Fig 1(e) and Fig 2, a potential field source surface model (PFSS)[16,17] was run using an ADAPT-GONG magnetogram[37-39] from November 21st, 2022, with a source surface height set to the canonical value of 2.5 R_S[18] via the the open source pfsspy[40] software. The footpoint mapping from PSP down to the solar surface followed the methodology[41] comprising a ballistic heliosphere[42,43] and the PFSS domain from 2.5R_S down to the photosphere.

The results for PSP E10 were distinct and compelling. As shown in Fig 1 and 2, for November 20 - November 21, PSP was rotating faster than the Sun and moving from left to right in the Carrington frame of reference shown in those plots. The footpoint mapping connected deep inside two mid-latitude negative polarity coronal holes of substantial area. This source mapping is uniquely well-supported as compared to prior PSP encounters owing to the comparison of the in situ data: Firstly, the magnetic polarity measured by PSP throughout the encounter well explained by the PFSS current sheet geometry and coronal hole polarity. Secondly, the times when PSP maps to the center of these large coronal holes correspond to maxima in solar wind speed, and at the time the connection switches from one source to another in the model there is a distinct dip in solar wind speed, clearly consistent with the traversal of overexpanded field lines at the coronal hole boundaries[44]. This correspondence is clearly shown in figure 1 where the transition between "Stream 1" and "Stream 2" marked in the bottom panel corresponds to the dip in solar wind speed (black trace, panel 3).

Supplementary: PSP/SWEAP data analysis

We use proton and alpha particle measurements from the Solar Wind Electrons Alphas and Protons (SWEAP) instrument suite[10] on Parker Solar Probe. The proton spectrum in Fig 4 is taken from the SPAN-Ion SF00 data product, averaged over the time range 2021-11-20/04:00:00 - 2021-11-20/19:00:00 and summed over all look directions. We work in units of energy flux as opposed to number flux or distribution function as it results in a spectrum spanning fewer orders of magnitude at high energy, facilitating the comparison between SPAN-Ion and ISOIS/Epi-Lo data, as well as being the quantity most directly related to the SPAN-Ion measurements. The power law for the protons is fit to the four highest energy SPAN data points and the ISOIS data points. The alpha spectrum is obtained in the same way from SPAN-Ion's sf01 data product, except that a small amount (~1%) of contaminant protons leaking in from the sf00 channel are accounted

for and subtracted. The large shift to higher energy of the alphas relative to the protons during this interval means that the contaminant protons have no impact on the power law part of the spectrum or its exponent, and only affect the lowest energy data points.

Supplementary: Reconnection magnetic field

The strength of the magnetic field that drives interchange reconnection will control the rate of magnetic energy release as well as the spectra of energetic particles produced. While the SDO/HMI observations reveal the structure of the magnetic field in the low corona, these measurements do not reveal the strength of the magnetic field that is actually undergoing reconnection since there is substantial variation of the field strength along the surface. To estimate the strength of the magnetic field driving the flow bursts measured by PSP, we project the measured magnetic field at PSP and project this magnetic field down to the solar surface. The radial magnetic field B_R at perihelion of E10 as shown in Figure 1 is around 600nT. Direct measurements of the radial profile of B_R over the PSP orbits have established an R^{-2} scaling for the field, consistent with the conservation of the radial magnetic flux. However, deviations from this scaling are expected close to the sun. Specifically, because closed flux occupies a substantial fraction of the solar surface, the open flux will be compressed into a reduced fraction of the solar surface which will lead to greater compression of the magnetic field near the solar surface. A rough estimate of the increased magnetic field compression can be obtained by averaging the radial magnetic field obtained from the PFSS model during the E10 perihelion. The radial dependence of this averaged field is shown in Figure S1. The magnetic field compression from $2.5R_s$, the outer boundary of the PFSS grid, down to just above the solar surface is around 26, which is well above the compression of around 6.25 from the R^{-2} dependence. Thus, we assume that the R^{-2} describes the radial dependence from R = $13.4R_s$ to $2.5R_s$ and take the compression of 26 from $2.5R_s$ to just above the solar surface. The projection of the 600nT field down to the solar surface is around 4.5G, which is in reasonable agreement with the strength of the solar surface magnetic field shown in Figure 2.

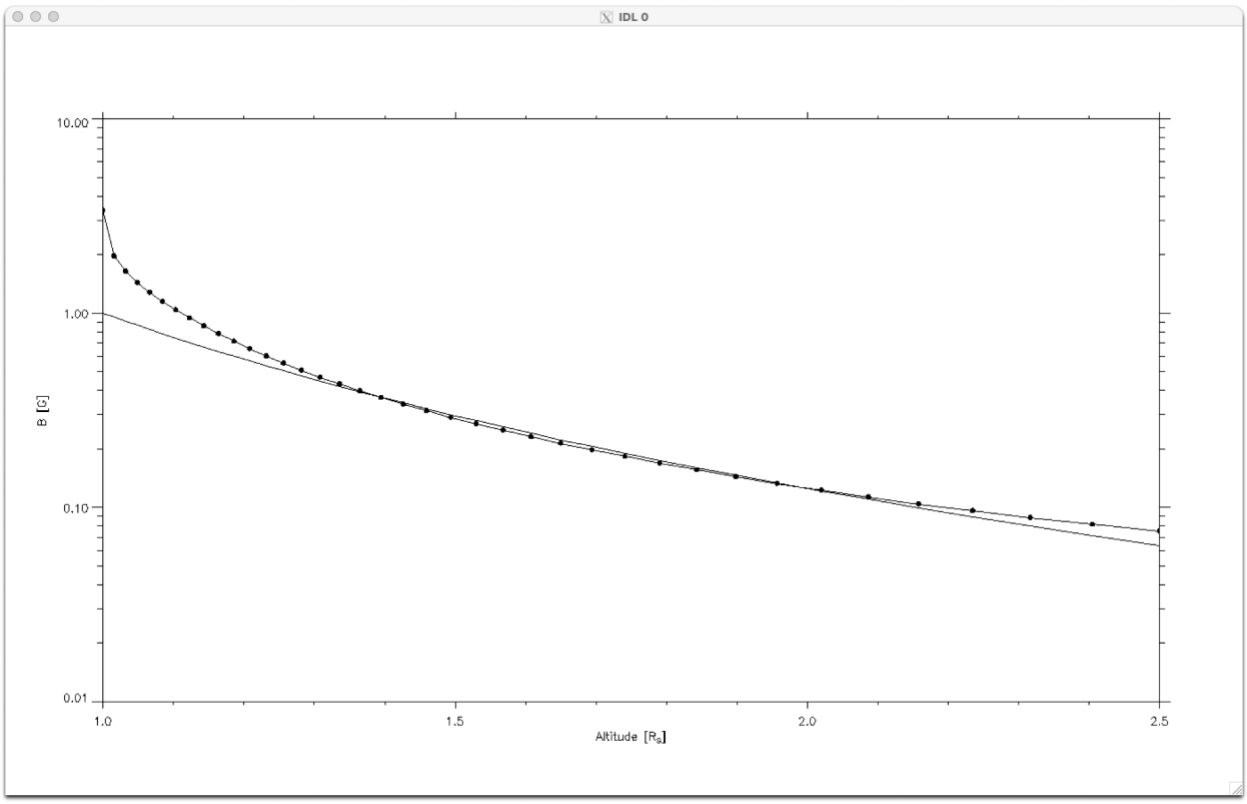

Supplementary: PIC simulations

Our estimate of the rate of interchange reconnection based on projections of the PSP observations back to the low corona suggest that reconnection there is deeply in the collisionless regime. To explore the structure of the interchange reconnection exhaust and the resulting energetic proton and alpha spectra measured at by PSP, we use the particle-in-cell (PIC) model p3d[45]. The MHD model is not adequate to explore the particle energization documented in the PSP data. We limit the calculations to a 2D system with an initial magnetic geometry that leads to reconnection between open and closed flux low in the corona[46]. Because of constraints on the domain size possible with the PIC model, there is no gravity in the simulations so the model does not describe the complete dynamics of the solar wind drive mechanism. In addition, line-tied boundary conditions are not imposed at the nominal coronal surface. Thus, the model is not a complete description of interchange reconnection in the low corona but will provide information on the dynamics of collisionless reconnection, the structure of the outflow exhaust and the spectra of accelerated particles. We include alpha particles (5% by number) so that the spectra of protons and alphas can be compared.

The initial state for the simulation consists of a band of vertical flux (field strength B_0 in the negative radial direction) with a low plasma density ($0.1n_0$) and an adjacent region with higher density that is a cylindrical equilibrium. The detailed initial state has been described previously[34] so the governing equations are not repeated here. The peak magnetic field of the cylindrical equilibrium is $0.76B_0$ with a peak density of n_0. The temperatures are uniform with $T_e = T_p = T_a =$

$0.06 m_p V_{A0}^2$ with V_{A0} the Alfven speed based on B_0, n_0 and the proton mass m_p. Thus, in the initial state the plasma pressure is small compared with the magnetic pressure as expected in the corona. The guide field B_z is nonzero everywhere except in the region with vertical flux and is chosen to balance the pressure and tension forces. The peak value of B_z is $1.09B_z$ at the center of the region of cylindrical flux. The vertical and cylindrical field slightly overlap in the initial state and have opposite directions so that reconnection quickly onsets.

The results of the simulation are presented in normalized units: times to the Alfven transit time across the domain of scale length L, L/V_{A0}, plasma fluxes to $n_0 V_{A0}$ and energies to $m_p V_{A0}^2$ The domain dimensions in the x and y directions are equal. The mass ratio $m_p/m_e = 25$ is artificial as is the velocity of light ($20V_{A0}$) and the proton inertial scale $d_p = L/163.84$. As has been established in earlier papers, the results are not sensitive to these values[29]. The radius of the cylindrical magnetic field is $60d_p$ and the grid scales are $0.02d_p$ in both space directions, with around 400 particles per cell.

Because the velocities and energies in the simulation are normalized to the Alfven speed V_{A0} and $m_p V_{A0}^2$, respectively, direct comparison with the observations require that these parameters, and specifically the Alfven speed V_{A0} where reconnection is taking place, be established. As described in the text of the paper, we use two distinct approaches for estimating V_{A0}. The first comes from the amplitude of the flow bursts measured by PSP at $13.4R_s$, which have values around 300km/s. The second comes from comparing the proton spectra from the simulation and that measured with SPANi. Specifically, we equate the low energy limit of the proton powerlaw spectrum from the simulation and the observations. This yields $m_p V_{A0}^2$ = 1.4keV, which corresponds to V_{A0} = 370km/s. Thus, the two approaches yield comparable values, which enables us to directly compare the simulation results with the observations. Of course, the spectral indices of around -7 for the spectral indices of the proton and alpha energy fluxes from the simulation are independent of this normalization. That they are in approximate agreement with the observational data is strong support for the interchange reconnection model for these energetic particles. We further note that a simulation with half of the domain size ($L=81.92d_p$) produced powerlaw spectra with similar spectral indices.

References for Supplementary Material only

37. Arge, C. N. et al, Air Force Assimilative Photospheric Flux Transport (ADAPT) Model, AIP confererence proceedings, 1216, 1, 343 (2010).
38. Arge, C. N. et al., Improving data drivers for coronal and solar wind models, J. Phys., CS-444 (2011).
39. Arge, C. N. et al., Modelinig the corona and solar wind using ADAPT maps that include far-side observations, Solar Wind 13 conference proceedings, CS-1539 (2013).
40. Stansby, D, A. Yeates, and S. Badman, pfsspy: A Python package for potential source surface modeling, J. Open Source Software, 5, 2732 (2020).
41. Badman, S. T. et al., Magnetic connectivity of the Ecliptic plane within 0.5 au: potential field source surface modeling of the first Parker Solar Probe encounter, Astrophys. J. Supp., 246, 23 (2020).

42. Nolte, J. T. and E. C. Roelof, Large-scale structure of the interplanetary medium, I: High coronal source longitude of the quiet-time solar wind, Solar Phys., 33, 241 (1973).
43. MacNeil, A. R. et al., A statistical evaluation of ballistic backmapping for the slow solar wind: The interplay of solar wind acceleration and corotation, MNRAS, 10.1093 (2021).
44. Wang, Y.-M. and N. R. Sheeley Jr., Solar wind speed and coronal flux-tube expansion, Astrophys. J., 355, 726 (1990).
45. Zeiler, A, et al., Three-dimensional particle simulations of collisionless magnetic reconnection, J. Geophys. Res., 107, 1230 (2002).
46. Fisk, L. A., The open magnetic flux of the Sun. I. Transport by reconnections with coronal loops, Astrophys. J., 636, 563 (2005).